Chemistry & Biology
Article

A Sensitive and Quantitative Technique for Detecting Autophagic Events Based on Lysosomal Delivery

Hiroyuki Katayama,[1,2] Takako Kogure,[2] Noboru Mizushima,[3] Tamotsu Yoshimori,[4,5] and Atsushi Miyawaki[1,2,*]
[1]Life Function and Dynamics, ERATO, JST
[2]Brain Science Institute, RIKEN, 2-1 Hirosawa, Wako-city, Saitama 351-0198, Japan
[3]Department of Physiology and Cell Biology, Tokyo Medical and Dental University Graduate School and Faculty of Medicine, 1-5-45 Yushima, Bunkyo-ku, Tokyo 113-8519, Japan
[4]Department of Genetics, Graduate School of Medicine
[5]Laboratory of Intracellular Membrane Dynamics, Graduate School of Frontier Bioscience
Osaka University, Suita, Osaka 565-0871, Japan
*Correspondence: matsushi@brain.riken.jp
DOI 10.1016/j.chembiol.2011.05.013

SUMMARY

We sought to develop a sensitive and quantitative technique capable of monitoring the entire flux of autophagy involving fusion of lysosomal membranes. We observed the accumulation inside lysosomal compartments of Keima, a coral-derived acid-stable fluorescent protein that emits different-colored signals at acidic and neutral pHs. The cumulative fluorescent readout can be used to quantify autophagy at a single time point. Remarkably, the technique led us to characterize an autophagy pathway in *Atg5*-deficient cells, in which conventional LC3-based autophagosome probes are ineffective. Due to the large Stokes shift of Keima, this autophagy probe can be visualized in conjunction with other green-emitting fluorophores. We examined mitophagy as a selective autophagic process; time-lapse imaging of mitochondria-targeted Keima and GFP-Parkin allowed us to observe simultaneously Parkin recruitment to and autophagic degradation of mitochondria after membrane depolarization.

INTRODUCTION

Macroautophagy, often referred to simply as autophagy, is mediated by a special organelle termed the autophagosome (Klionsky and Ohsumi, 1999; Mizushima, 2007). During starvation-induced autophagy in mammals, the C terminus of microtubule-associated protein light chain 3 (LC3) is lipidated; the membrane-bound form (LC3-II) is recruited to both the inner and outer surfaces of autophagosomes. EGFP-LC3, a fusion of LC3 and EGFP (a bright variant of *Aequorea* GFP), is considered to be a good early marker of autophagic events (Figures 1A and 1B) (Kabeya et al., 2000; Mizushima et al., 2001). Upon starvation of cells stably expressing EGFP-LC3, EGFP fluorescence becomes punctate due to the membrane localization of this fusion protein. In these cells, autophagosomes usually appear as fluorescent dots or ring-shaped structures. Then, as autophagosomes fuse with lysosomes to generate autolysosomes (Baba et al., 1994), the EGFP fluorescence is attenuated by two distinct mechanisms. LC3-II on the outer membrane is delipidated, returning to the cytosolic pool of free LC3 (Kabeya et al., 2004). LC3-II on the inner membrane is degraded by lysosomal proteases; the majority of the chimeric EGFP is degraded or irreversibly acid quenched in autolysosomes (Tanida et al., 2005). In vivo mammalian autophagy has been successfully studied using mice bearing an EGFP-LC3 transgene (Mizushima et al., 2010).

However, LC3-based probes have several limitations. First, these probes are only detected transiently during the process of autophagy. To detect fluorescence in a sensitive and quantitative manner, it is necessary to perform time-lapse imaging over a long time interval, with significantly high temporal resolution to observe this transient event; high-throughput assay systems that acquire fluorescence images at a single time point may miss autophagosome formation. Second, uncertainties remain concerning the behavior of LC3 on autophagosomes (Figures 1A and 1B). To our knowledge, it is not known how LC3-II is distributed on autophagosomes, or what the proportions of molecules are on the outer and inner membranes. Furthermore, the timing of the delipidation of outer membrane LC3-II during autophagy is unclear (Figure 1A or 1B). Kimura et al. (2007) incorporated into EGFP-LC3 an additional monomeric red fluorescent protein (mRFP) that is resistant to both acid and lysosomal proteases. The resulting chimeric protein (mRFP-EGFP-LC3) produces sustainable red and transient green fluorescence, serving as a valuable tool with which to investigate the complex regulation of autophagosome to autolysosome conversion. However, because both mRFP and EGFP are fused to LC3, the red and green fluorescence intensities may be affected by intramolecular resonance transfer or other unidentified factors that would hinder the interpretation of studies examining autophagy. Third, it has also been reported that LC3-based probes can produce false-positive signals due to probe aggregation or incorporation into intracellular protein aggregates (Kuma et al., 2007).

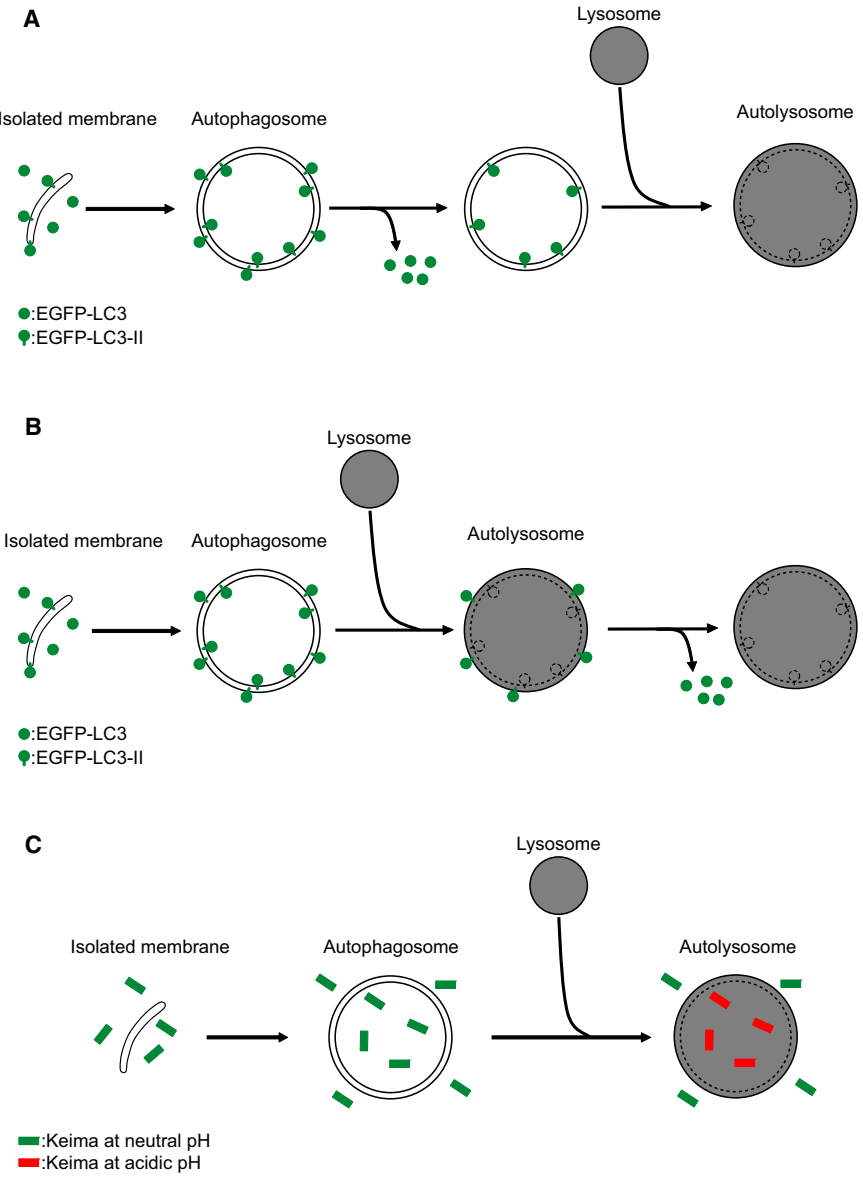

Figure 1. The Schematic Representation of the Detection of Autophagy with EGFP-LC3 or Keima Probes

Under starvation conditions, an isolated, cup-shaped membrane is formed and elongated. The double-membrane structure engulfs a portion of the cytoplasm to form an autophagosome. Subsequently, the autophagosome fuses with a lysosome to form an autolysosome. Acidic compartments are shown in gray.

(A and B) The membrane-bound form of LC-3 (LC3-II) is recruited to both the inner and outer surfaces of autophagosomes. When cells stably expressing EGFP-LC3 are starved, autophagosomes typically appear as fluorescent dots or ring-shaped structures. As these autophagosomes fuse with lysosomes to generate autolysosomes, the EGFP fluorescence in these structures is attenuated by two mechanisms. LC3-II on the outer membrane is delipidated and returns to the cytosolic pool of free LC3. LC3-II on the inner membrane is degraded by lysosomal proteases; the associated EGFP is degraded as well as irreversibly acid quenched within autolysosomes. The timing whereby LC3-II on the outer membrane undergoes delipidation is different between (A) and (B).

(C) A fluorescent protein derived from coral, Keima, changes color upon conversion of an autophagosome to an autolysosome. Although EGFP-LC3 can be used as an autophagosome marker, Keima-based probes can record the formation of autolysosomes and, thus, provide a cumulative fluorescent readout of autophagic activities.

RESULTS AND DISCUSSION

Autophagy Probes that Sense Autophagosome/Lysosome Fusion and Stably Accumulate within Autolysosomes

In this study we focused on the formation of autolysosomes. Autophagosomal fusion with lysosomes exposes intra-autophagosomal contents to both acidic pH and proteases. We sought to develop a probe that could monitor autolysosome maturation by employing a fluorescent protein resistant to lysosomal proteases that exhibits a reversible change in color in response to acidic pH (Figure 1C). This pH-dependent change in fluorescence would allow the protein to track the conversion of autophagosomes to autolysosomes. We developed such a fluorescent protein that is highly stable within autolysosomes, providing a cumulative readout of autophagic activity in the absence of complex time-lapse imaging. Because the probe does not depend on LC3 modification, this method can monitor the flux of autophagy on a cellular level in a more comprehensive manner than that performed in LC3-associated systems (Mizushima et al., 2010).

Among coral proteins that are resistant to lysosomal proteases (Katayama et al., 2008), we considered several that emitted different-colored signals at acidic and neutral pHs. After accounting for individual pH dependence and color, we selected monomeric and dimeric versions of Keima, mKeima, and dKeima, respectively (see Figure S1 available online) (Kogure et al., 2006). Keima has an emission spectrum that peaks at 620 nm and a bimodal excitation spectrum peaking at 440 and 586 nm corresponding to the neutral and ionized states of the chromophore's phenolic hydroxyl moiety, respectively (Violot et al., 2009). pH titration experiments confirmed that the neutral and ionized states predominate at high and low pHs, respectively, with a pKa value of 6.5 (Figures 2A and 2B). This paradoxical pH dependence was also observed for the fluorophores ratiometric pHluorin (R-pHluorin) (Miesenböck et al., 1998) and the related fast-maturing mutant iR-pHluorin (Figure 2C). Dual-excitation ratiometric pH measurements can be performed using mKeima (550/438), dKeima (550/438), or iR-pHluorin (481/390) (Figure 2D). Although iR-pHluorin

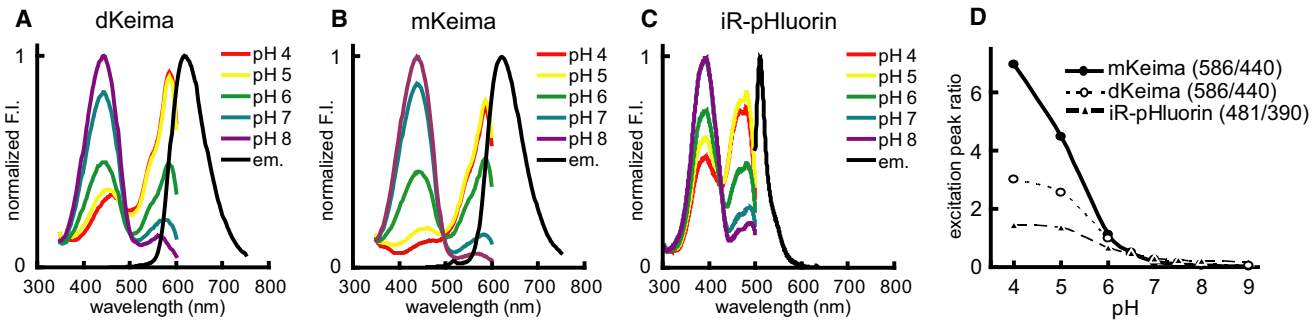

Figure 2. pH-Dependent Spectral Properties of dKeima, mKeima, and iR-pHluorin

(A–C) We measured the fluorescence excitation and emission spectra of purified recombinant proteins to determine the pH dependence of the excitation spectra of dKeima (A), mKeima (B), and iR-pHluorin (C). (D) pH titration curves of the excitation peak ratio of dKeima (586/440), mKeima (586/440), and iR-pHluorin (481/390). F. I., fluorescence intensity.

was completely degraded by lysosomal proteases at acidic pH, mKeima and dKeima were resistant to acid proteases (Figures S2A and S2B). Thus, transfection of mKeima or dKeima into mammalian cells results in the formation of bright punctate structures with a high ratio of excitation at 550/438 nm. Because dKeima matures slightly faster than mKeima (data not shown), we chose dKeima to characterize these punctate structures further. We examined the appearance of mouse embryonic fibroblast (MEF) cells transfected with dKeima under different culture conditions (Figure 3A). Fluorescent structures appeared when cells were treated with 200 nM rapamycin or underwent starvation by culture in Hank's balanced salt solution (HBSS). The starvation-induced appearance of these structures was blocked by treatment with PI3 kinase inhibitors (10 mM 3-methyladenine [3-MA] or 100 nM Wortmannin), inhibitors of V-type H^+-ATPase (100 nM Bafilomycin A1), or H^+-ionophores (30 mM NH_4Cl). These results indicate that a high ratio of excitation at 550/438 nm for intracellular dKeima reflects autolysosome formation.

Use of Keima-Based Probes with Other Green-Emitting Fluorophores

Because it possesses a long wavelength emission that peaks at 620 nm, Keima can be simultaneously imaged with green-emitting fluorophores within the same cell without serious concern for cross-excitation, cross-detection, and resonance transfer (Figure S3). We cotransfected dKeima and iR-pHluorin into MEF cells. Dual-excitation ratio imaging using dKeima, but not iR-pHluorin, revealed punctate structures with high ratio values and were sensitive to NH_4Cl treatment (Figure 3B).

Although dual-excitation ratiometric dyes are excited alternately at two different wavelengths, fluorophore emission is collected at a single fixed wavelength; the pair of intensity measurements must be collected sequentially. This limitation makes dual-excitation ratiometric imaging generally inadequate to follow rapid events in highly motile structures. In this regard, the observation of autolysosome formation using dKeima may be limited by the poor spatiotemporal resolution of conventional wide-field microscopy.

To confirm that the punctate structures were lysosomes, we examined costaining with a lysosomal marker. To distinguish these intracellular structures, we had to increase z axis resolution. In addition, because lysosomes are often motile, we sought to increase the rapidity of production and collection of excitation peak ratios. Although we had previously established a special laser-scanning confocal microscopy (LSCM) system in which two laser beams alternately scanned every line to achieve dual-excitation ratiometric imaging (Shimozono et al., 2002; Fukano et al., 2008), the same function is now available on certain commercial LSCM systems. In this study, we examined dKeima-expressing MEF cells by confocal imaging using a Zeiss LSM 510 META system equipped with a multi-argon laser (458, 488, and 514.5 nm) and a He/Ne laser (543 nm) (Figure S4). Prior to imaging, we treated cells with an Alexa 488-conjugated dextran for 6 hr to identify lysosomes. Cells were then scanned on each line sequentially by the 458 and 543 nm lasers and the 488 nm laser to detect red emissions, providing the confocal ratio (543/458) images for dKeima, and green emissions, generating confocal images of lysosomes (Figure 3C). In a separate experiment using this microscopy system, we generated a pH titration curve using a dKeima-containing solution (Figure 3D). The ratio (543/458) reflecting an acidic environment (pH <6.0) was 1.5–3.0. We then determined that the ratio (543/458) for pH <6.0 (Figure 3C, red) corresponded to the signals for lysosomal staining using the fluorescent dextran (Figure 3C, green).

Detection of Autolysosome and Autophagosome Formation by a Keima-Based Probe and EGFP-LC3, Respectively

We transfected dKeima into MEF cells stably expressing EGFP-LC3, then monitored the resultant fluorescence to observe autophagic events (Figure 4). After starving for 1 hr in HBSS, transfected cells developed cytoplasmic punctate structures with high ratio (550/438) signals derived from dKeima fluorescence. These signals, indicating autolysosome formation, increased cumulatively over time. After replacement of HBSS with fresh growth medium, dKeima-derived fluorescence persisted in almost all transfected cells. In contrast, EGFP-LC3 fluorescence increased during starvation but quickly decreased to normal levels after substitution of rich medium, confirming the detection of autophagosome formation by LC3-based probes.

Visualizing Parkin-Dependent Delivery of Impaired Mitochondria to Lysosomes

Although autophagy was originally thought to be a nonspecific form of lysosomal degradation, recent findings indicate that

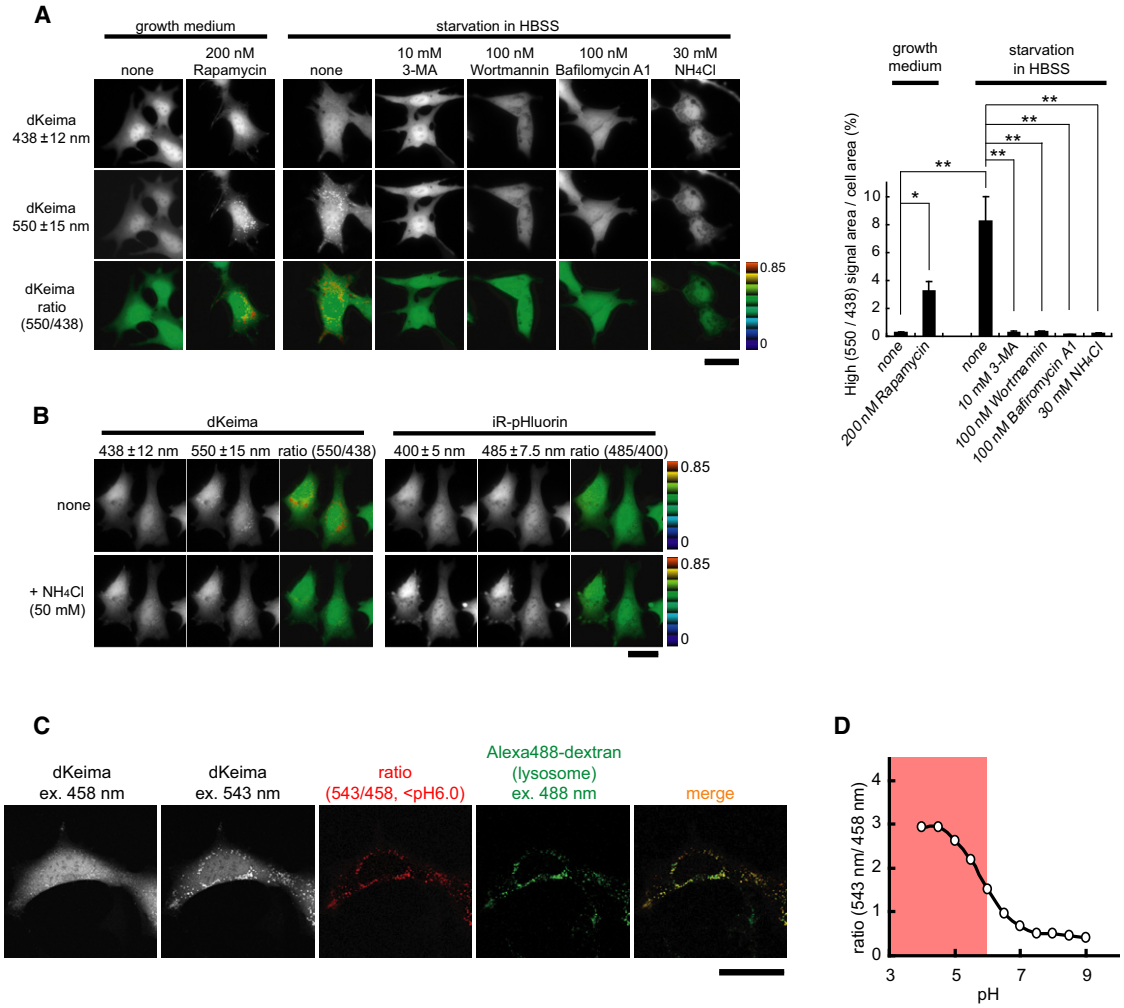

Figure 3. Dual-Excitation Ratiometric Imaging of Autolysosomes Using the Coral-Derived Fluorescent Protein Keima

dKeima fluorescence was evoked using two excitation filters (438 ± 12 nm and 550 ± 15 nm) and a 610LP emission filter (see Figure S3A), whereas iR-pHluoin fluorescence was obtained using two excitation filters (400 ± 5 nm and 485 ± 7.5 nm) and an emission filter (535 ± 17.5 nm) (see Figure S3C).

(A) dKeima is delivered to lysosomes via an autophagic process. Left view shows dKeima-expressing MEF cells incubated for 4 hr in either growth or starvation medium (HBSS), then imaged. We examined the effects of rapamycin containing normal medium or HBSS containing 3-MA, Wortmannin, Bafilomycin A1, or NH_4Cl (each image was acquired after a 4 hr incubation). High ratio (550/438) signals, which originate from low pH compartments (lysosomes), are shown as red. Scale bar represents 20 μm. Right view illustrates the proportion of the high ratio (550/438) signal area (red) to the total cellular area in 30 transfected cells calculated for each experiment. Data represent the mean ± SD of three independent experiments. *$p < 0.05$, **$p < 0.02$.

(B) Double dual-excitation ratiometric imaging of dKeima and iR-pHluorin in MEF cells. MEF cells expressing both dKeima and iR-pHluorin were imaged after incubation for 4 hr in starvation medium (HBSS). After obtaining an initial set of images (top panels), 50 mM NH_4Cl was added to neutralize the lysosomal lumen before acquiring a second set (bottom panels). Scale bar represents 20 μm.

(C) Confocal imaging demonstrating the colocalization of high ratio dKeima signals and lysosomal marker signals in punctate structures. An MEF cell expressing dKeima was treated with Alexa 488-dextran for 6 hr, then each line was sequentially scanned with the 458 and 543 nm lasers to detect dKeima and the 488 nm laser to detect Alexa 488-dextran, as shown in Figure S4. Signals representing the acidic compartment (pH <6.0) and lysosomes are shown in red and green, respectively. Colocalization between dKeima and Alexa 488-dextran signals was calculated to be 82.8% ± 6.0% (n = 5). Scale bar represents 20 μm.

(D) A pH titration curve using a dKeima-containing solution.

autophagy includes a selective component (Bjørkøy et al., 2005; Pankiv et al., 2007). In mammalian cells the ubiquitin ligase Parkin (Shimura et al., 2000) is selectively recruited to dysfunctional mitochondria exhibiting low membrane potentials to mediate their autophagosomal engulfment and subsequent degradation (Narendra et al., 2008, 2009). To visualize the process by which impaired mitochondria are delivered to lysosomes, we engineered a form of mKeima to localize to the matrix of mitochondria (mt-mKeima) by fusing a tandem repeat of the COX VIII presequence to mKeima. We chose mKeima because of its larger responses to pH changes than dKeima (Figure 2D). mt-iR-pHluorin was also constructed for reference. We enhanced the specificity of the mitochondrial localization of these constructs by including on/off control of transcription. Because MEF cells

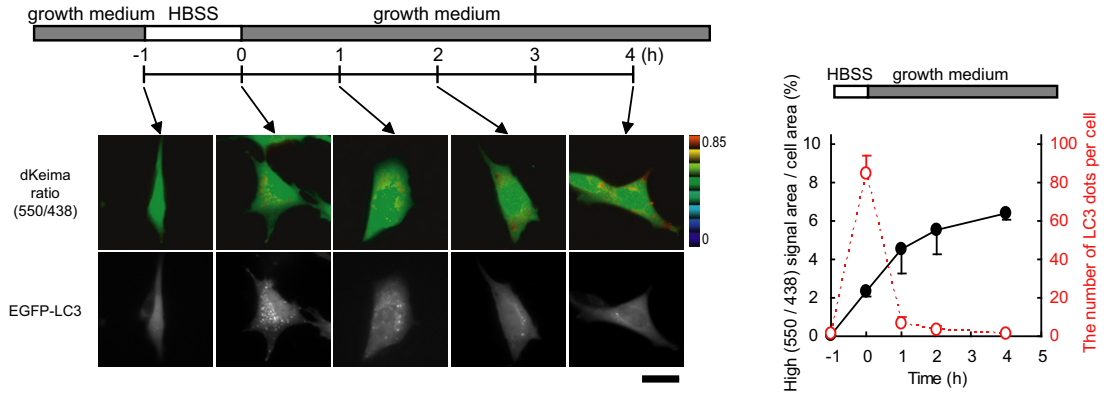

Figure 4. Cumulative Detection of Autophagy Using dKeima

MEF cells stably expressing EGFP-LC3 were maintained in growth medium after transfection with dKeima cDNA. dKeima fluorescence was obtained using two excitation filters (438 ± 12 nm and 550 ± 15 nm) and a 610LP emission filter (see Figure S3A). EGFP signals were visualized using a 470 ± 10 nm excitation filter and a 517.5 ± 22.5 nm emission filter (see Figure S3D). Cells were starved in HBSS for 1 hr, then recultured in growth medium. Left images were acquired at the beginning (−1 hr) and end (0 hr) of the starvation period as well as after the growth medium was replaced (1, 2, and 4 hr). Scale bar represents 20 μm. Right view shows the proportion of the high ratio (550/438) signal area (red) to the total cellular area in 30 transfected cells (black solid circles) and the number of EGFP-LC3-positive aggregates per cell (red open circles) plotted over time. Data represent the mean ± SD of three independent experiments.

produce only low levels of Parkin, we transfected these cells with Parkin cDNA. After cotransfection with cDNAs for Parkin and mt-mKeima or mt-iR-pHluorin, MEF cells were treated with Ponasterone A for 24 hr to induce transient gene expression of the mitochondrially targeted fluorophores. After incubation in growth medium for 12 hr, mt-mKeima and mt-iR-pHluorin clearly localized to mitochondria. Subsequent treatment with DMSO (vehicle) for 24 hr did not generate high ratio signals for either mt-mKeima (550/438) or mt-iR-pHluorin (485/400), indicating the absence of mitophagy (Figure 5A). After treatment of cells with CCCP (a mitochondrial uncoupler) and oligomycin (an ATP synthase inhibitor), the two probes displayed different readouts. After depolarizing mitochondria for 24 hr with the aforementioned inhibitors, cells exhibited punctate structures throughout the cytoplasm displaying strong signals for mt-mKeima at an excitation wavelength of 550 nm. The representative image (Figure 5B) indicates that a large fraction of mitochondria was delivered to lysosomes scattered throughout the cell. In contrast, the subpopulation of mitochondria containing mt-mKeima that exhibited strong fluorescence at 438 nm was distributed close to the nucleus. The ratio (550/438) image clearly demonstrates a differential distribution of intact (green) and degraded (red) mitochondria (Figure 5B, left, top). When lysosomes were neutralized by the addition of 50 mM NH_4Cl, the ratio (550/438) values for all mitochondria returned to prestimulus levels (Figure 5B, left, bottom). In contrast, fluorescence for mt-iR-pHluorin was observed only in intact mitochondria. Because neutralization with 50 mM NH_4Cl did not regenerate mt-iR-pHluorin-derived fluorescence in lysosomes, it is likely that the majority of mt-iR-pHluorin was completely degraded by lysosomal proteases (Figure 5B, right panels).

After pretreating MEF cells expressing mt-mKeima with Alexa 488-dextran for 6 hr, we subjected samples to incubation with CCCP and oligomycin. Cells were then examined by confocal imaging using a Zeiss LSM 510 META system (Figure S5). Confocal ratio (543/458) images of mt-mKeima and a confocal image of the lysosomes revealed the colocalization of mitochondrially targeted fluorophore to lysosomes (Figure 5C). We generated a pH titration curve using an mKeima-containing solution to determine that a ratio (543/458) of 1.2–4.0 reflected an acidic environment (pH <6.0) (Figure 5D). Our data demonstrate that the ratio (543/458) signals corresponding to a pH less than 6.0 (Figure 5C, red) matched those for lysosomal staining (Figure 5C, green).

Time-Lapse Imaging of Mitophagy and Parkin Recruitment in MEF Cells

To observe Parkin recruitment to autophagosomes and the autophagic degradation of mitochondria, we cotransfected EGFP-Parkin and mt-mKeima into MEF cells. The time courses for these two events within single cells were determined by time-lapse imaging over an 18 hr incubation in CCCP and oligomycin (Figure 6A; Movie S1). Initially, EGFP-Parkin was localized diffusely throughout the cell; there were no mitophagy-specific signals. After 2 hr, punctate structures containing EGFP emerged, indicating that EGFP-Parkin had been recruited to impaired mitochondria. Subsequently, high ratio (550/438) signals from mt-mKeima began to appear and accumulate. After 10 hr, EGFP-Parkin fluorescence began to decrease, suggesting that the fusion protein had been delivered to autolysosomes and degraded. In contrast, high ratio (550/438) fluorescence derived from mKeima increased as a function of time. After 18 hr, a large-field image was acquired in a region of heterogeneous EGFP-Parkin expression (Figure 6B). Of three cells within this region, only the cell that expressed EGFP-Parkin exhibited high ratio (550/438) mKeima-derived fluorescence (Figure 6B, white arrowhead). The proportion of high ratio (550/438) signal area to total mitochondrial area was increased only in Parkin-expressing cells that had been treated with CCCP and oligomycin (Figure 6C), demonstrating the Parkin-dependence of mitophagy in MEF cells.

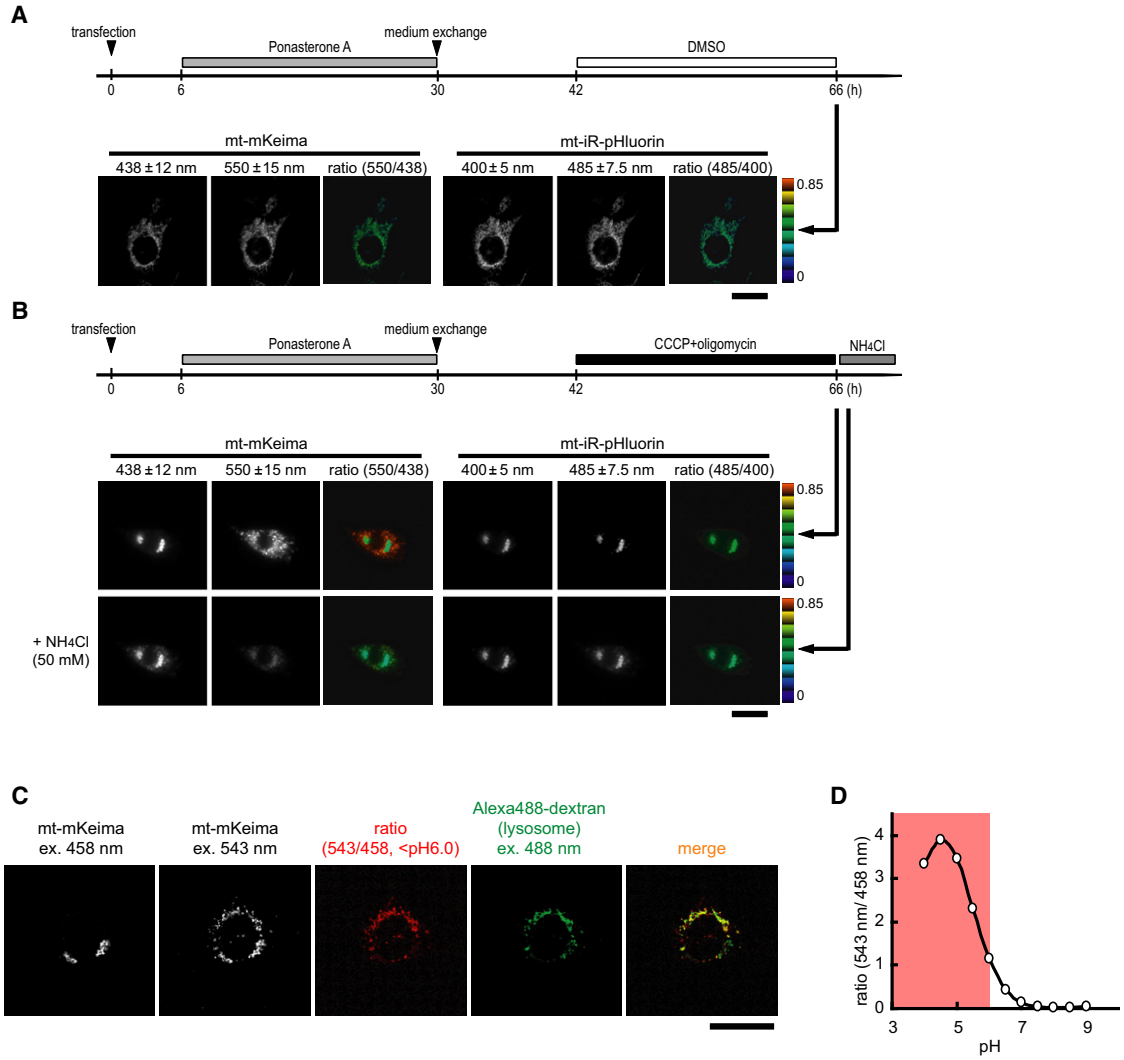

Figure 5. Cumulative Detection of Mitophagy Using Mitochondrially Targeted mKeima

(A and B) Double dual-excitation ratiometric imaging of mt-mKeima and mt-iR-pHluorin in Parkin-overexpressing MEF cells. mt-mKeima and mt-iR-pHluorin gene expression was induced for 1 day prior to experimentation by the addition of 1 μM Ponasterone A. mt-mKeima was imaged as described for dKeima in Figures 3 and 4 (see Figure S3B), whereas mt-iR-pHluorin was imaged as described for iR-pHluorin in Figure 3 (see Figure S3C). Scale bars represent 20 μm. Cells were imaged following a 24 hr treatment with (A) DMSO (vehicle alone) or (B) 30 μM CCCP and 1 μg/ml oligomycin. After initial images were obtained (top panels), a second set of images was obtained after the addition of 50 mM NH_4Cl to neutralize the lysosomal lumen (bottom panels). Similar imaging results were obtained in three independent experiments.

(C) Confocal imaging to examine the colocalization of punctate structures showing high ratio mt-mKeima signals and lysosomal marker signals. MEF cells expressing mt-mKeima were incubated with Alexa 488-dextran for 6 hr, then treated for 1 day with 30 μM CCCP and 1 μg/ml oligomycin. Cells were sequentially scanned on each line using the 458 and 543 nm lasers for mt-mKeima and the 488 nm laser for Alexa 488-dextran, as shown in Figure S5. Signals for the acidic compartment (pH <6.0) and for lysosomes are shown in red and green, respectively. Yellow signals indicate colocalization of lysosomes with high ratio mt-mKeima signals. Colocalization between mt-mKeima and Alexa 488-dextran signals was calculated to be 86.5% ± 4.7% (n = 4). Scale bar represents 20 μm.

(D) A pH titration curve using an mKeima-containing solution.

Autophagy Observed in *Atg5*-Deficient Cells

Recently, a new form of macroautophagy has been discovered, which is not suppressed by abrogation of ubiquitin-like protein systems like Atg5 (Nishida et al., 2009). Although it was previously believed that mammalian macroautophagy required several *Atg* genes, autophagosomes/autolysosomes can be observed by electron microscopy (EM) in embryonic fibroblasts from *Atg5*-deficient mice ($Atg5^{-/-}$ MEFs). We also detected high levels of autophagy in *Atg5*-deficient cells using dKeima (Figures 7A–7C). Interestingly, autophagy-specific signals in $Atg5^{-/-}$ MEFs were observable even when the cells were not under starvation conditions (Figure 7A). This Atg5-independent pathway is not detected using LC3-based autophagosome probes because LC3 cannot be modified in the absence of Atg5 (Figure 7C, right, bottom). Thus, dKeima allows us to study autophagy in a more comprehensive manner than that performed in LC3-associated systems.

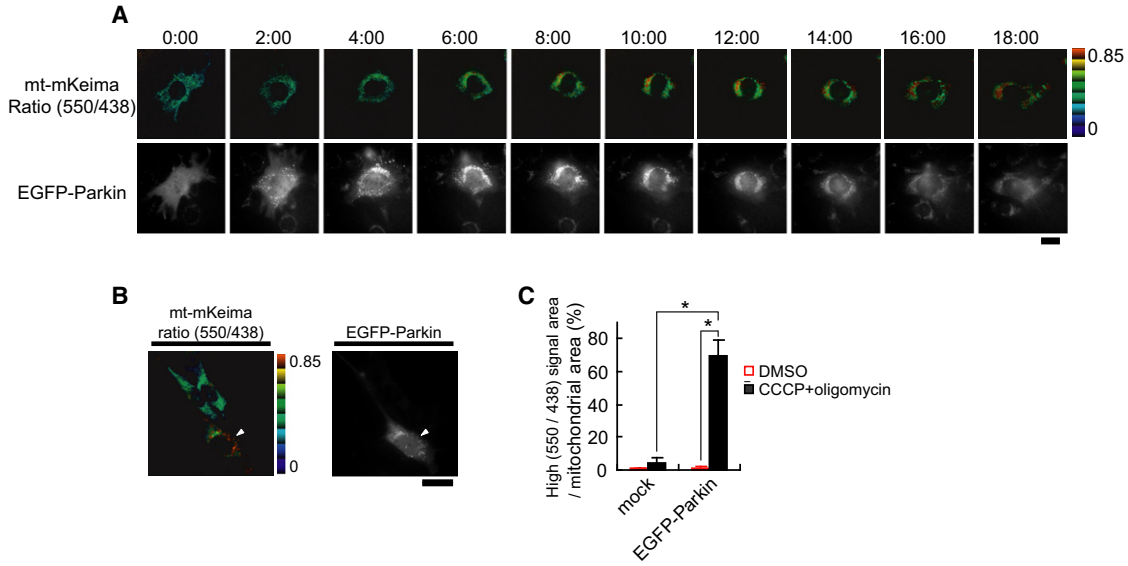

Figure 6. Simultaneous Observation of EGFP-Parkin and mt-mKeima in MEF Cells

After the induction of mt-mKeima expression for 1 day by the addition of 1 μM Ponasterone A, mt-mKeima and EGFP-Parkin were imaged as described in Figure 5 (see Figures S3B and S3D).

(A) Time-lapse imaging of mitophagy (top) and Parkin recruitment (bottom) in MEF cells. Scale bar represents 20 μm. See also Movie S1.

(B) Large-field image of three MEF cells examining mitophagy (left) and Parkin recruitment (right); the cell undergoing mitophagy is indicated by a white arrowhead. Scale bar represents 20 μm.

(C) mt-mKeima-expressing MEF cells were transfected with the EGFP-Parkin cDNA or mock vector. Samples were then treated with DMSO (open bar) or 30 μM CCCP and 1 μg/ml oligomycin (solid bar) for 24 hr before imaging. The proportion of the high ratio (550/438) signal area (red) to the total mitochondrial area served as an index of mitophagy. Each experiment examined 30 transfected cells. Data represent the mean ± SD of three independent experiments. *$p < 0.01$.

Interestingly, our results exploring Atg5-independent autophagy differed from those of Nishida et al. (2009); their observation examined autophagosomes and autolysosomes by EM or by quantification of lysosomal protein (LAMP-2) immunofluorescence. They determined that macroautophagy was sensitive to brefeldin A (BFA) and dependent on Rab9 function, suggesting that late endosomes and vesicles derived from the *trans*-Golgi were involved in autophagosome formation. However, we doubt that an EM- or LAMP-2-dependent method can provide sufficiently quantitative data. Our experiments using dKeima were able to quantify autophagy in *Atg5*-deficient cells, leading us to conclude that neither BFA (Figure 7D) nor Rab9 deficiency (Figure 7E) abrogates autophagy. The disparity between this report and previous results questions which types of autophagy are detected by dKeima.

There are three types of autophagy: macroautophagy, microautophagy, and chaperone-mediated autophagy (CMA). Macroautophagy is characterized by fusion of lysosomal membranes with the autophagosome. Microautophagy involves inward invagination of lysosomal membranes. By contrast, CMA does not involve substantial changes in lysosomal membrane; instead, cytosolic proteins that are unfolded by chaperone proteins translocate directly across the lysosomal membrane. According to its mechanism of action, dKeima is expected to sense all types of macroautophagy and microautophagy (Sahu et al., 2011). However, it is unlikely that the probe senses CMA (Dice, 2007) because Keima lacks the KFERQ-like motif required for inclusion into the CMA pathway. In addition, suppression of PI3 kinase activity by treatment with 3-MA or LY294002 (Figure 7F) or by siRNA-mediated downregulation of Beclin 1 (Figure 7G) abolished dKeima fluorescence, despite the independence of CMA from PI3 kinase enzymatic activity. Finally, dKeima fluorescence was not affected by the silencing of LAMP-2A or Hsc70 (Figure 7G), despite the requirement of these molecules for CMA.

These results indicate that the autophagy observed in *Atg5*-deficient cells is dependent on Beclin 1 or PI3 kinase activity. Further studies with knockdown and pharmacological inhibition experiments are underway to explore the mechanisms underlying this pathway.

Quantitative Observation of the Process of a Single Autophagic Event

To develop a probe to detect autolysosome formation, Rosado et al. (2008) constructed pH-insensitive RFP combined with a pH-sensitive GFP; the resultant probe, Rosella, was successfully used in yeast cells to follow autophagic engulfment of both cytosol and specific organelles. Upon entering vacuoles, the green signal was abolished, whereas the red signal remained. The authors attributed these results to the differential pH sensitivity of RFP and GFP but did not examine the sensitivity of Rosella to proteases. Probes generated by tandem fusion of two fluorescent proteins generally display several problems; the red-to-green signal ratio of Rosella may be affected by differential maturation rates, fluorescence resonance energy transfer, and proteolytic cleavage between the two proteins. In contrast, Keima-based probes possess a single fluorophore, reproducibly giving rise to the same ratio values under varying conditions,

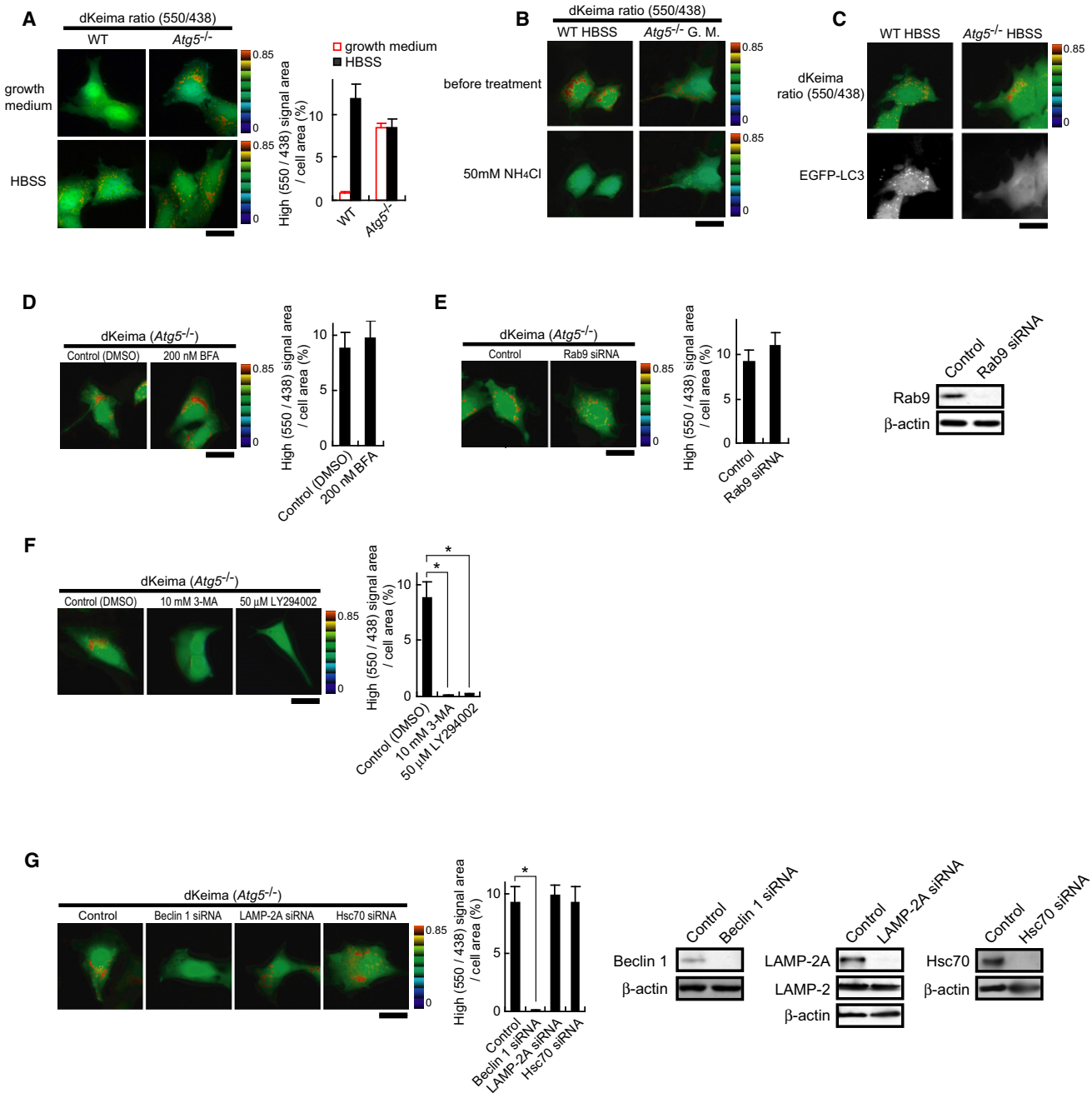

Figure 7. Cumulative Detection and Quantitative Characterization of Autophagy Using dKeima in *Atg5*-Deficient Cells

(A) Two days after transfection with the cDNA encoding dKeima, WT and *Atg5*$^{-/-}$ MEF cells were incubated for 4 hr in growth or starvation medium (HBSS), then imaged. Left view shows representative images. Right view shows statistics. We analyzed the incidence of autophagy statistically by calculating the proportion of the high ratio (550/438) signal area (red) to the total cellular area in 30 transfected cells per experiment. Data represent the mean ± SD of three independent experiments.

(B) After an initial set of images was obtained (top panels) as in (A), additional images were acquired after 50 mM NH_4Cl was added to neutralize the lysosomal lumen (bottom panels). G. M., growth medium.

(C) Simultaneous observation of EGFP-LC3 and dKeima in WT and *Atg5*$^{-/-}$ MEF cells stably expressing EGFP-LC3 under starvation conditions.

(D–G) Dual-excitation ratiometric imaging of dKeima in starving *Atg5*$^{-/-}$ MEF cells after treatment with 200 nM BFA (D), Rab9 siRNA (E), 10 mM 3-MA or 50 μM LY294002 (F), or siRNAs specific for Beclin 1, LAMP-2A, or Hsc70 (G). In each experiment the incidence of autophagy was statistically analyzed by calculating the proportion of the high ratio (550/438) signal area (red) to the total cellular area in 30 transfected cells. Data represent the mean ± SD of three independent experiments. *$p < 0.01$. To evaluate the effects of individual siRNAs, cell lysates were prepared and analyzed by immunoblotting using antibodies against Rab9 (E), Beclin 1 (G), LAMP-2A (LAMP-2) (G), or Hsc70 (G). Scale bars represent 20 μm.

ensuring that autophagy can be quantitatively measured. It should be noted that all color bars accompanying ratio images in this paper represent the same correspondence to ratio (550/438) values.

Although autophagy was originally considered a bulk degradation process induced by starvation, recent evidence indicates that autophagy has selective properties that respond to a variety of homeostatic systems. These processes have attracted much research because substantial evidence indicates that deregulated lysosomal degradation leads to a variety of diseases (Eskelinen et al., 2003; Komatsu et al., 2006; Nixon et al., 2008). Although EGFP-LC3 can function as an autophagosome marker, Keima-based probes provide a record of autolysosome formation, thus providing a cumulative fluorescent readout of autophagic activity. This readout can be used to quantify autophagy at a single time point, making this technique amenable to high-throughput screening. However, this technique cannot be applied to fixed cell samples where the pH gradient across lysosomal membranes is lost. The fusion of Keima to specific cytosolic proteins or targeting of this probe to specific organelles can also create multiple Keima-based probes that can be used to explore the selective aspects of autophagy. In this study, we targeted the monomeric version of Keima (mKeima) to mitochondria to quantitatively monitor mitophagy induced by the depolarization of mitochondrial membranes and to determine the requirement for Parkin recruitment.

Importantly, the technologies described in this paper do not dispute the usefulness of EGFP-LC3 as an imaging tool but only indicate that Keima-based probes can be used in a complementary manner to examine the entirety of autophagic events (Figure 4).

SIGNIFICANCE

Considerable progress has been made toward understanding the biochemical mechanisms underlying the formation of autophagosomes. Currently, probes to evaluate cellular autophagosomal processes utilize the combination of microtubule-associated protein light chain 3 (LC3) and fluorescent proteins, such as GFP-LC3. However, these probes only identify early events in autophagy. A type of macroautophagy has recently been discovered, which is not inhibited by silencing ubiquitin-like protein systems, such as those requiring Atg5. A critical limitation to studies of autophagy has been the inability to monitor Atg5-independent macroautophagy by conventional LC3-based autophagosome probes because LC3 is not modified in this pathway. We designed a probe that would allow us to study autophagy in a more comprehensive framework. To develop a sensitive and quantitative technique to observe the flux of autophagy involving lysosomal fusion on a cellular level over time, we focused on detecting the fusion of autophagosomes with lysosomes. Upon delivery to lysosomes, cytosolic components and organelles encapsulated by autophagosomes are exposed to acidic pH and lysosomal proteases. We have previously demonstrated that several fluorescent proteins derived from corals retain fluorescence in these harsh environments. Among the proteins is Keima, which is endowed with a large Stokes shift. Keima emits different-colored signals at acidic and neutral pHs, providing a cumulative readout of autophagic activities. We performed dual-excitation ratiometric imaging by localizing Keima to either the cytoplasm or mitochondria to monitor starvation-induced autophagy and membrane depolarization-induced mitophagy, respectively. These systems allowed us to obtain a quantitative characterization of Atg5-independent autophagy and to explore the mechanisms underlying this pathway.

EXPERIMENTAL PROCEDURES

Gene Construction and Mutagenesis

iR-pHluorin was generated by introducing four mutations (F46L, F64L, S72A, and M153T) into R-pHluorin. Site-directed mutations were introduced as described (Sawano and Miyawaki, 2000). The cDNA encoding dKeima, mKeima, or iR-pHluorin was cloned into $pRSET_B$ (Invitrogen) for bacterial expression or into pCS2 for mammalian expression. The cDNA encoding the tandem repeat of the mitochondrial-targeting sequence of COX VIII (Rudolf et al., 2004) was amplified using primers containing 5′-KpnI and 3′-BamHI sites, and the digested product was cloned with a BamHI-EcoRI fragment for mKeima or iR-pHluorin into the KpnI/EcoRI sites of pIND(SP1) (Invitrogen) to generate mt-mKeima/pIND(SP1) or mt-iR-pHluorin/pIND(SP1), respectively. Mouse Parkin was cloned from mouse brain cDNA. cDNA encoding Parkin was amplified using primers containing 5′-HindIII and 3′-EcoRI sites, and the digested product was cloned into the HindIII/EcoRI sites of pcDNA3 (Invitrogen).

Protein Expression

Recombinant fluorescent proteins with a polyhistidine tag at N terminus were expressed in *Escherichia coli* (JM109(DE3)) and purified as described (Nagai et al., 2001).

pH Titration

Fluorescent proteins were examined in a series of buffers with pHs ranging from 4 to 9 using SPEX Fluorolog-3 (HORIBA) or LSM 510 META system (Carl Zeiss).

In Vitro Protease Assay

Recombinant fluorescent proteins (0.1 mg/ml) were treated with lysosomal contents (0.1 mg/ml) in 125 mM KCl, 20 mM NaCl, 2 mM $CaCl_2$, and 2 mM $MgCl_2$ at pH 7.4 or 4.5. pH conditions were achieved using 25 mM HEPES-NaOH (pH 7.4) or acetate buffer (pH 4.5) as buffers. The sample mixtures were incubated at 37°C for 18 hr. Samples were analyzed either by SDS-PAGE after staining with Coomassie brilliant blue or by measurement of their fluorescence intensities after dilution with 100-fold 100 mM HEPES/NaOH (pH 8.0) containing 30 mM KCl and 120 mM sodium gluconate.

Cell Culture and Transfection

MEF cells from wild-type and *Atg5*-deficient mice were cultured on standard 35 mm glass-bottom dishes in Dulbecco's modified Eagle's medium (DMEM; Sigma) containing 5% fetal bovine serum (FBS) supplemented with 4 mM L-Glu. Cells were transfected with plasmid DNAs using Lipofectamine 2000 reagent (Invitrogen). To achieve expression of mitochondrially targeted fluorescent proteins, cells were cotransfected with pVgRXR (Invitrogen) in addition to mt-mKeima/pIND(SP1) or mt-iR-pHluorin/pIND(SP1) and given a pulse (24 hr) with Ponasterone A (Invitrogen) on the following day. After transfection with the plasmid DNA for EGFP-LC3, MEF cells stably expressing the chimeric protein were obtained through selection with G418.

Wide-Field Imaging

After removing samples from a normal CO_2 incubator, cells cultured on 35 mm glass-bottom dishes were incubated in HBSS (GIBCO) containing 15 mM HEPES-NaOH (pH 7.4). Samples were imaged using an inverted microscope (IX81; Olympus) equipped with a standard 75 W xenon lamp, a 40× objective lens (UplanFlN 40xOil, N.A. 1.30), and a cooled CCD camera (iXon EM+; Andor

Technology). For long-term imaging, 35 mm glass-bottom dishes were placed in a stage-top incubator (IBC chamber; Tokai Hit) and time-lapse imaged in phenol red-free DMEM containing 5% FBS. Multiple cubes accommodating appropriate excitation and emission filters and dichroic mirrors were automatically exchanged for multicolor and dual-excitation ratiometric imaging. The whole system was controlled using MetaMorph 7.6 software (Molecular Devices).

Quantification of Autophagy

Ratio (550/438) images of Keima were created and analyzed using MetaMorph 7.6 software. Ratio values ranged from 0 to 0.85 at all times. High ratio (550/438) regions were automatically segmented, and their areas were calculated. The whole-cell region was delineated manually on a fluorescent image to facilitate area calculation. The ratio (high ratio [550/438] area/total cell area) was used as an index of autophagic activity.

Confocal Imaging

Cells that had been loaded with Alexa 488-dextran (Molecular Probes) for 6 hr were subjected to confocal imaging using the LSM 510 META system (Carl Zeiss) equipped with a 40× objective lens (C-Apochromat 40×/1.20 W, N.A. 1.20), a multi-argon laser (458, 488, and 514.5 nm), and a He/Ne laser (543 nm). Proper alignment and correct image registration of the two laser lines and detection channels were verified using double-labeled fluorescent beads (TetraSpeck Fluorescent Microsphere Standards, 0.5 μm in diameter; Molecular Probes). Colocalization between Keima and Alexa 488 signals on confocal images was performed using the MetaMorph colocalization module. Individual experimental details are described in Figures S4 and S5.

RNAi

The following sequences were used in protein knockdown experiments:

mouse Rab9-siRNA sense, 5′-CGGCGACUAUCCUUACUUUTT-3′ and antisense, 5′-AAAGUAAGGAUAGUCGCCGTT-3′;
mouse Beclin 1-siRNA sense, 5′-GAGUUGCCGUUAUACUGUUCU-3′ and antisense, 5′-AACAGUAUAACGGCAACUCCU-3′;
mouse LAMP-2A-siRNA sense, 5′-GAGGAGUACUUAUUCUAGUGU-3′ and antisense, 5′-ACUAGAAUAAGUACUCCUCCC-3′;
mouse Hsc70-siRNA sense, 5′-CGAUGAAGCUGUUGCCUAUTT-3′ and antisense, 5′-AUAGGCAACAGCUUCAUCGGG-3′;
control-siRNA sense, 5′-CGAUUCGCUAGACCGGCUUCA-3′ and antisense, 5′-UGAAGCCGGUCUAGCGAAUCG-3′.

RNAi oligonucleotides were transfected into MEF cells by using Lipofectamine 2000 according to the manufacturer's protocols. After 2 days, cells were analyzed by western blotting or imaged as described above.

Antibodies

For western blotting analysis, we used the following antibodies: rabbit polyclonal anti-Rab9 (Abcam); rabbit polyclonal anti-Beclin 1 (MBL); rabbit polyclonal anti-LAMP-2A (Zymed Laboratories); rat monoclonal anti-LAMP-2 (Santa Cruz Biotechnology); and goat anti-Hsc70 (R&D Systems, Inc.).

Statistical Analysis

Statistical significance was determined using the paired Student's t test. A p value <0.05 was considered statistically significant.

SUPPLEMENTAL INFORMATION

Supplemental Information includes five figures and one movie and can be found with this article online at doi:10.1016/j.chembiol.2011.05.013.

ACKNOWLEDGMENTS

The authors thank RIKEN BSI-Olympus Collaboration Center for its technical assistance and Dr. D. Mou for critical comments. This work was supported in part by grants from the MEXT of Japan, Grant-in-Aid for Scientific Research on priority areas and KAKENHI 22700381, Molecular Ensemble Program at RIKEN, and the Human Frontier Science Program.

Received: February 25, 2011
Revised: May 25, 2011
Accepted: May 25, 2011
Published: August 25, 2011

REFERENCES

Baba, M., Takeshige, K., Baba, N., and Ohsumi, Y. (1994). Ultrastructural analysis of the autophagic process in yeast: detection of autophagosomes and their characterization. J. Cell Biol. *124*, 903–913.

Bjørkøy, G., Lamark, T., Brech, A., Outzen, H., Perander, M., Overvatn, A., Stenmark, H., and Johansen, T. (2005). p62/SQSTM1 forms protein aggregates degraded by autophagy and has a protective effect on huntingtin-induced cell death. J. Cell Biol. *171*, 603–614.

Dice, J.F. (2007). Chaperone-mediated autophagy. Autophagy *3*, 295–299.

Eskelinen, E.L., Tanaka, Y., and Saftig, P. (2003). At the acidic edge: emerging functions for lysosomal membrane proteins. Trends Cell Biol. *13*, 137–145.

Fukano, T., Shimozono, S., and Miyawaki, A. (2008). Development of microscopic systems for high-speed dual-excitation ratiometric Ca^{2+} imaging. Brain Cell Biol. *36*, 43–52.

Kabeya, Y., Mizushima, N., Ueno, T., Yamamoto, A., Kirisako, T., Noda, T., Kominami, E., Ohsumi, Y., and Yoshimori, T. (2000). LC3, a mammalian homologue of yeast Apg8p, is localized in autophagosome membranes after processing. EMBO J. *19*, 5720–5728.

Kabeya, Y., Mizushima, N., Yamamoto, A., Oshitani-Okamoto, S., Ohsumi, Y., and Yoshimori, T. (2004). LC3, GABARAP and GATE16 localize to autophagosomal membrane depending on form-II formation. J. Cell Sci. *117*, 2805–2812.

Katayama, H., Yamamoto, A., Mizushima, N., Yoshimori, T., and Miyawaki, A. (2008). GFP-like proteins stably accumulate in lysosomes. Cell Struct. Funct. *33*, 1–12.

Kimura, S., Noda, T., and Yoshimori, T. (2007). Dissection of the autophagosome maturation process by a novel reporter protein, tandem fluorescent-tagged LC3. Autophagy *3*, 452–460.

Klionsky, D.J., and Ohsumi, Y. (1999). Vacuolar import of proteins and organelles from the cytoplasm. Annu. Rev. Cell Dev. Biol. *15*, 1–32.

Kogure, T., Karasawa, S., Araki, T., Saito, K., Kinjo, M., and Miyawaki, A. (2006). A fluorescent variant of a protein from the stony coral Montipora facilitates dual-color single-laser fluorescence cross-correlation spectroscopy. Nat. Biotechnol. *24*, 577–581.

Komatsu, M., Kominami, E., and Tanaka, K. (2006). Autophagy and neurodegeneration. Autophagy *2*, 315–317.

Kuma, A., Matsui, M., and Mizushima, N. (2007). LC3, an autophagosome marker, can be incorporated into protein aggregates independent of autophagy: caution in the interpretation of LC3 localization. Autophagy *3*, 323–328.

Miesenböck, G., De Angelis, D.A., and Rothman, J.E. (1998). Visualizing secretion and synaptic transmission with pH-sensitive green fluorescent proteins. Nature *394*, 192–195.

Mizushima, N. (2007). Autophagy: process and function. Genes Dev. *21*, 2861–2873.

Mizushima, N., Yoshimori, T., and Levine, B. (2010). Methods in mammalian autophagy research. Cell *140*, 313–326.

Mizushima, N., Yamamoto, A., Hatano, M., Kobayashi, Y., Kabeya, Y., Suzuki, K., Tokuhisa, T., Ohsumi, Y., and Yoshimori, T. (2001). Dissection of autophagosome formation using Apg5-deficient mouse embryonic stem cells. J. Cell Biol. *152*, 657–668.

Nagai, T., Sawano, A., Park, E.S., and Miyawaki, A. (2001). Circularly permuted green fluorescent proteins engineered to sense Ca^{2+}. Proc. Natl. Acad. Sci. USA *98*, 3197–3202.

Narendra, D., Tanaka, A., Suen, D.F., and Youle, R.J. (2008). Parkin is recruited selectively to impaired mitochondria and promotes their autophagy. J. Cell Biol. *183*, 795–803.

Narendra, D., Tanaka, A., Suen, D.F., and Youle, R.J. (2009). Parkin-induced mitophagy in the pathogenesis of Parkinson disease. Autophagy *5*, 706–708.

Nishida, Y., Arakawa, S., Fujitani, K., Yamaguchi, H., Mizuta, T., Kanaseki, T., Komatsu, M., Otsu, K., Tsujimoto, Y., and Shimizu, S. (2009). Discovery of Atg5/Atg7-independent alternative macroautophagy. Nature *461*, 654–658.

Nixon, R.A., Yang, D.S., and Lee, J.H. (2008). Neurodegenerative lysosomal disorders: a continuum from development to late age. Autophagy *4*, 590–599.

Pankiv, S., Clausen, T.H., Lamark, T., Brech, A., Bruun, J.A., Outzen, H., Øvervatn, A., Bjørkøy, G., and Johansen, T. (2007). p62/SQSTM1 binds directly to Atg8/LC3 to facilitate degradation of ubiquitinated protein aggregates by autophagy. J. Biol. Chem. *282*, 24131–24145.

Rosado, C.J., Mijaljica, D., Hatzinisiriou, I., Prescott, M., and Devenish, R.J. (2008). Rosella: a fluorescent pH-biosensor for reporting vacuolar turnover of cytosol and organelles in yeast. Autophagy *4*, 205–213.

Rudolf, R., Mongillo, M., Magalhães, P.J., and Pozzan, T. (2004). In vivo monitoring of Ca($^{2+}$) uptake into mitochondria of mouse skeletal muscle during contraction. J. Cell Biol. *166*, 527–536.

Sahu, R., Kaushik, S., Clement, C.C., Cannizzo, E.S., Scharf, B., Follenzi, A., Potolicchio, I., Nieves, E., Cuervo, A.M., and Santambrogio, L. (2011). Microautophagy of cytosolic proteins by late endosomes. Dev. Cell *20*, 131–139.

Sawano, A., and Miyawaki, A. (2000). Directed evolution of green fluorescent protein by a new versatile PCR strategy for site-directed and semi-random mutagenesis. Nucleic Acids Res. *28*, E78.

Shimozono, S., Fukano, T., Nagai, T., Kirino, Y., Mizuno, H., and Miyawaki, A. (2002). Confocal imaging of subcellular Ca^{2+} concentrations using a dual-excitation ratiometric indicator based on green fluorescent protein. Sci. STKE *2002*, pl4.

Shimura, H., Hattori, N., Kubo, S., Mizuno, Y., Asakawa, S., Minoshima, S., Shimizu, N., Iwai, K., Chiba, T., Tanaka, K., and Suzuki, T. (2000). Familial Parkinson disease gene product, parkin, is a ubiquitin-protein ligase. Nat. Genet. *25*, 302–305.

Tanida, I., Minematsu-Ikeguchi, N., Ueno, T., and Kominami, E. (2005). Lysosomal turnover, but not a cellular level, of endogenous LC3 is a marker for autophagy. Autophagy *1*, 84–91.

Violot, S., Carpentier, P., Blanchoin, L., and Bourgeois, D. (2009). Reverse pH-dependence of chromophore protonation explains the large Stokes shift of the red fluorescent protein mKeima. J. Am. Chem. Soc. *131*, 10356–10357.

